Numerical Simpson's Rule for Real Time and Accurate T2* maps generation Using 3D Quantitative GRE

C. Fatnassi[1, 2], R. Boucenna[2] and H. Zaidi[3]

[1]Faculty of Biology and Medicine, University of Lausanne, Lausanne, Switzerland
[2]Radio-oncology Department, Hirslanden, Lausanne, Switzerland
[3]Department of Nuclear Medicine and Molecular Imaging, Geneva University Hospital, Geneva, Switzerland

Abstract— **T2* plays an important role in the quantitative evaluation of brain function and tissue iron content. Conventional approaches for quantitative T2* maps generation use linear or nonlinear least square curve fitting. Nevertheless, these methods are very time consuming and could not be used in real time T2* computation. Hagberg et al (2002) proposed a numerical method that relies on trapezoidal integration of signal decay. This method is faster than conventional methods and provides an accurate T2* value. However, this approach is valid for small echo spacing and low noise level. In this work, we propose an alternative numerical integration relying on Simpson's rule that generates an accurate T2* maps even in the presence of large echo spacing and high noise value. The proposed method yields T2* values comparable to NumART2* in the presence of small echo spacing and high SNR and provides better results in the opposite case.**

Keywords— **GRE, Quantitative T2*, Real time, Numerical computation.**

I. Introduction

Quantitative magnetic resonance imaging (MRI) by means of T2* relaxometry is becoming an increasingly requested tool in many areas of MR imaging. The effective transverse relaxation rate R2*(1/T2*) characterizes static magnetic field variations on the mesoscopic level [1], which can be associated with local concentrations of paramagnetic macromolecules that may reveal the physiology of disordered brain function [2]. It is applied for BOLD contrast studies [3, 4] as well as for the assessment of iron content in the brain [5], heart [6], and liver [7], dynamic susceptibility contrast MRI [8, 9], cerebral venous blood volume measurement [10] and brain abnormalities detection, such as multiple sclerosis [11]. Quantitative T2* maps can be generated using different approaches, the golden standard being the nonlinear least square signal decay fitting approach. T2* can be also generated using a linear fit of the signal decay after putting it in logarithmic scale. However, the above mentioned methods based on curve fitting are time consuming and their use in real time T2* quantification remains a challenge. In 2002, Hagberg et al. [12] introduced a numerical method, referred to as NumART2* to compute the T2* maps based on trapezoidal numerical integration. This method generates T2* maps with good accuracy and can be used in real time computation. However, the trapezoidal integration relies on linear approximation of signal decay between two echoes. This approximation remains valid for small echo spacing and noise free signal. In this work, we propose an alternative numerical method that overcomes the limitations of NumART2* in the presence of large echo spacing and high noise level. The method is based on Simpson's rule which combines trapezoidal and midpoint rule approximations to better interpolate the signal decay between echoes. The proposed method is then compared to the non-least square fit (exponential), linear least square fit and NumART2* using simulated and *in vivo* human studies.

II. Theory

A. Numerical Integration

The MRI signal in a 3D gradient echo experiment for a given n[th] voxel, assuming ideal signal decay in the absence of macroscopic field inhomogeneity can be described as follows in the time domain:

$$S_n(TE_N) = S_{0,n} \exp(-\frac{TE_N}{T2^*}) \quad (1)$$

where $S_n(TE_N)$ is the MR signal at a given echo time TE_N, S_0 is the magnetization at TE = 0 and T2* is the effective transverse relaxation time. In order to compute the area under the signal curve, we calculate the integral of the signal over echo times:

$$\int_{TE1}^{TEN} S_n(TE_N)\, dTE = \int_{TE1}^{TEN} S_{0,n} \exp\left(-\frac{TE_N}{T2} *\right) dTE \quad (2)$$

The integral of the left hand side can be approximated using Simpson's rule, which corresponds to the three-point Newton-Cotes quadrature rule:

D.A. Jaffray (ed.), *World Congress on Medical Physics and Biomedical Engineering, June 7-12, 2015, Toronto, Canada*,
IFMBE Proceedings 51, DOI: 10.1007/978-3-319-19387-8_27

$$\int_{TE1}^{TEN} S_n(TE_N)\,dTE = \frac{1}{6}(TE_N - TE_1)[S_n(TE_1) + S_n(TE_N) + 4S_n\left(\frac{TE_1+TE_N}{2}\right)] \quad (3)$$

Assuming fixed echo spacing, Simpson's rule uses a smooth quadratic interpolation between signal points and approximates well the signal decay in case of big time spacing between echoes. The right hand equation can be calculated analytically and by combining the 2 integrals, the T2* can be computed using the following approximation:

$$T^*_{2,n} = \frac{\frac{1}{6}(TE_N - TE_1)[S_n(TE_1)+S_n(TE_N)+4S_n\left(\frac{TE_1+TE_N}{2}\right)]}{S_n(TE_1) - S_n(TE_N)} \quad (4)$$

B. Correction of odd even artifact due to the bipolar gradient echo

More recent sequence implementations collect all echoes in one TR [13, 14], significantly reducing the required scan time. "Unipolar" approaches acquire all echoes using the same gradient polarity [15], while "bipolar" approaches provide more efficient acquisitions with data collected during both positive and negative gradient lobes [14]. Bipolar methods may account for phase errors that may result from eddy currents and gradient delays which can differ for positive and negative gradient lobes, disrupting the inter-echo phase consistency if the image voxel contains more than one tissue type. This problem may lead to the appearance of ringing artifact in the brain magnitude data (Fig. 4) and consequently, ringing artifacts appear in the computed T2* if numerical integration is used. The bipolar gradient is composed from 'in' and 'out' phase echoes. If the magnitude signal modulation is known, it can be removed by post-processing. Assuming the image voxel contains two types of tissues 1 and 2; The In-phase (IP) and Out-phase (OP) echo signal can be described as follows:

$$S_{n_{IP}}(TE_N) = \left(e^{\left(-R^*_{2,1}TE_{IP}\right)}\rho 1 + e^{\left(-R^*_{2,2}TE_{IP}\right)}\rho 2\right)e^{(i2\pi\varphi TE_{IP})} \quad (5)$$

$$S_{n_{OP}}(TE_N) = \left(e^{\left(-R^*_{2,1}TE_{OP}\right)}\rho 1 - e^{\left(-R^*_{2,2}TE_{OP}\right)}\rho 2\right)e^{(i2\pi\varphi TE_{OP})} \quad (6)$$

From the previous equations, the signal modulation between echoes can be computed as:

$$S_{Mod}(\%) = 100 \cdot \frac{(S_{n_{IP}}(TE_N) - S_{n_{OP}}(TE_N))}{2S_{n_{IP}}(TE_N)} \quad (7)$$

The modulation fraction can be removed from the In-phase and Out-phase magnitude signal by a simple subtraction as shown in the following equations:

$$S_{n_{IP_{Corr}}}(TE_N) = S_{n_{IP}}(TE_N) + S_{Mod} \cdot S_{n_{IP}}(TE_N) \quad (8)$$

$$S_{n_{OP_{Corr}}}(TE_N) = S_{n_{OP}}(TE_N) - S_{Mod} \cdot S_{n_{OP}}(TE_N) \quad (9)$$

III. Materials and Methods

To test our hypothesis and methods, we developed a numerical phantom using customized Matlab scripts (Mathworks, USA). We used simulated brain MRI data (Montreal Neurological Institute, Canada), which provide anatomical images segmented into disjoined special masks or templates (one per tissue type). The MR brain properties T1, T2* and PD (grey matter, white matter and CSF) were set to mimic our real brain data and used to simulate the magnitude signal of multi gradient echo sequence using an analytical solution to the Bloch equation:

$$S_n(TE_N) = \frac{M_{n,0}\exp(-TE_N/T_2{}^*)\sin(\alpha)(1-\exp(-TR/T_1))}{1-\cos(\alpha)\exp(-TR/T_1)} \quad (10)$$

where $M_{n,0}$ is the ideal signal free from field gradient inhomogeneities and α is the flip angle. To evaluate the T2* computation method in more details and in a wider range than the experimental condition; a total of 60 echoes were simulated using the following sequence parameters: TR/ flip angle = 50ms/ 10° and 1mm^2 in-plane resolution and matrix size of 256×256. The echo times were incremented to obtain the following values: 0.3/0.6/0.9/1.2/1.8 of the ratio TE/T2*. In order to assess the accuracy of the proposed approach as a function of noise, we introduce a random noise which depends on the simulated magnitude image SNR in such a way that the signal-to-noise ratio in the simulated data deteriorates with increasing echo time. In addition, the simulated model takes into account the partial volume effect which is caused by the presence of more than one substance within the same pixel. It also takes into account the macroscopic field inhomogeneities near the air/tissue interfaces to mimic *in vivo* data. T2* values were evaluated using NumART2*, linear least square fit and nonlinear least square fit (expo). The accuracy of the T2* computation using the different methods is calculated as follows:

$$Accuracy\ \% = 100 - 100 \cdot \left(\frac{(NumT2^* - T2^*)}{T2^*}\right) \quad (11)$$

where NumT2* is computed using the mentioned approaches and T2* is the value used in the simulation mimicking the *in vivo* studies (WM/GM/CSF/fat/muscle/skin = 61/70/50/58/30/58ms). *In vivo* studies were obtained from 20 human subjects using the acquisition protocol mentioned below. In order to assess the performance of the four methods for generating the T2* maps, an offline generation of T2* was realized. All scans were performed on a 3T Magnetom Trio MRI (Siemens Healthcare, Erlangen, Germany) using 32-channel phased-array coil. *In vivo* data were acquired using a 3D bipolar multi gradient echo sequence. 32 echoes were acquired with α/TR/TE1/ΔTE = 8°/47/1.23/1.23ms, 1.6 mm^3 isotropic resolution and a matrix size of 136×136×112, Grappa parallel imaging with acceleration factor of 2 and phase partial Fourier sampling factor of 6/8.

IV. Results and Discussion

As shown in Fig. 1, in the presence of low noise level and small echo spacing (ΔTE/T2*) < 0.2), the T2* maps were well generated by all methods with a slight overestimation when using NumART2*. When the echo spacing increases (ΔTE/T2*) > 0.2), NumART2* tends to overestimate the T2* values, although the accuracy is well maintained while using Simpson's rule, linear and NLLS fit. These results can be explained by the quadratic interpolation of signal decay between the echoes that Simpson's rule uses to approximate the area under the signal decay rather than a linear approximation that NumART2* uses. Increasing the echo spacing is equivalent to undersampling the echo number which is used to compute the T2* maps. Consequently, reducing the number of echoes diminishes the precision of T2* computation when using NumART2*. Simpson rule, linear and NLLS fit remain insensitive to the echo spacing or echo number sampling. Fig. 2 illustrates the accuracy of T2* computation as a function of noise levels present in the simulated data. For low noise level (<15%), all methods provide results with high accuracy, especially when generating T2* maps with Simpson's rule, linear and NLLS fit. NumART2* starts to diverge when the noise level becomes significant (>15%) and the T2* values are overestimated. However, Simpson's rule, linear and NLLS fit remain insensitive to added noise and, as such, the accuracy remains steady.

Simpson's rule combines two approximation methods to compute the signal integral, the midPoint and trapezoidal rules, which NumART2* is relying upon. This combination allows Simpson's rule to approximate well the signal decay between tow echo points using a smooth quadratic interpolation even in the presence of high noise level, thus providing accurate T2* maps. In other words, Simpson's rule plays the role of noise filter while approximating noisy signal decay. Fig. 3 compares the accuracy of T2* generated using the mentioned approaches (ROI drawn in the center of the brain). Linear fit computes T2* with high accuracy but remains the slowest approach. Simpson's rule combined with odd even correction overestimates T2* by about 2% against 4% for NumART2*.

The odd even modulation correction is shown in Fig. 4; (A&C) show the magnitude image and the T2* map without modulation correction. One can notice that the ringing artifacts is clearly present near the brain edges in both magnitude and T2* images. (B&D) show the data after modulation correction where the ringing artifact is well removed from both magnitude and T2* images without any spatial resolution loss (e.g. when using filters).

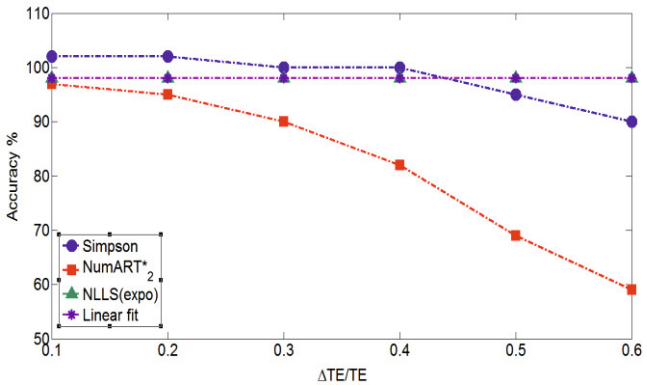

Fig 1. Dependence of T2* generation methods accuracy on echo intervals.

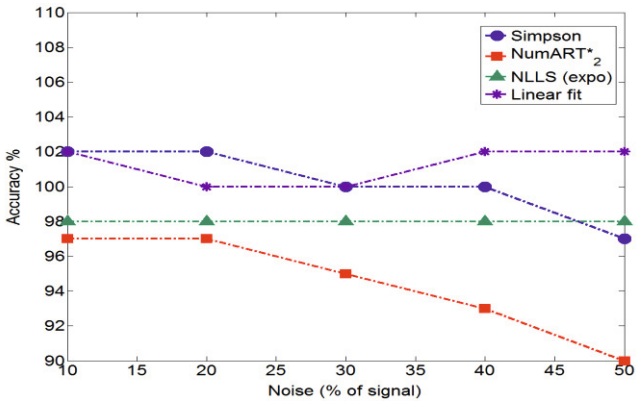

Fig 2. Dependence of T2* generation accuracy on noise levels.

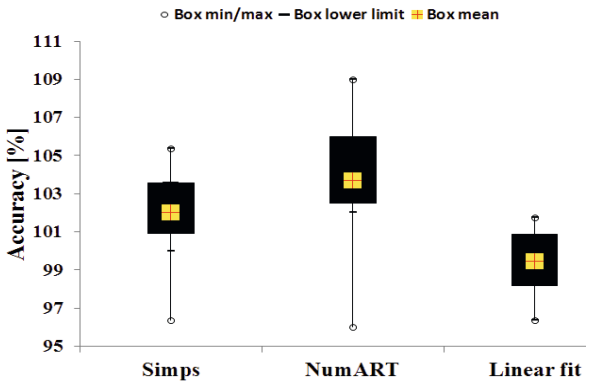

Fig 3. Accuracy of T2* generation methods compared to NLLS fit (expo).

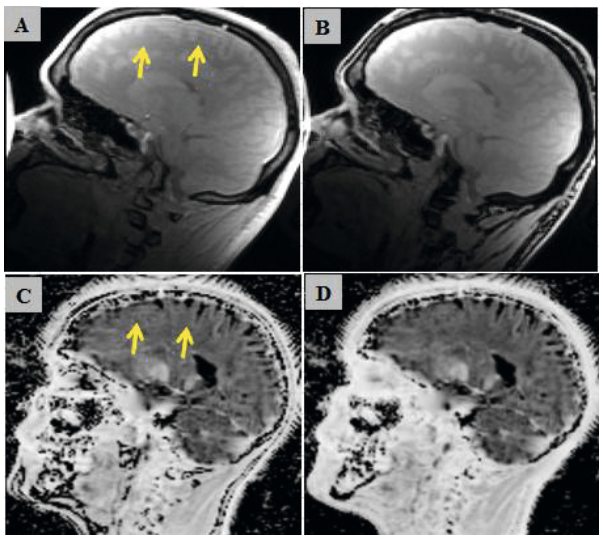

Fig 4. Upper row shows GRE data (A-B) without and with modulation correction, respectively. Lower row (C-D) shows the corresponding T2* maps. Arrows show ringing artifacts near the brain edges.

V. Conclusion

We proposed an alternative T2* maps generation which relies on Simpson's rule to approximate the geometric area under the signal decay. This approach combines two different approximations, namely midpoint and Trapezoidal rules that NumART2* relies upon. The method allows rapid whole brain mapping of T2* with a high accuracy even in the presence of large echo spacing or high noise level. The smooth quadratic interpolation, that Simpson's rule uses to approximate the signal decay between echoes, enables to yield accurate quantitative T2* values comparable to NLLS fit. Both simulation and *in vivo* studies showed that the proposed approach remains insensitive to noise level and time spacing between echoes. Therefore, undersampling the echoes number or low SNR would not diverge the T2* computation compared to NumART2*.

References

1. Dimitriy A. Yablonskiy et al. (2012) Voxel Spread functon Method for correction of magnetic field inhomogeneity Effects in Quantitative gradient Echo based MRI. Magn Reson Med 70:1283–1292.
2. Sammet S et al. (2010) Postprocessing correction for distortions in T2* decay caused by quadratic cross slice B0 inhomogeneity. Magn Reson Med 63:1258-1268.
3. Van der Zwaag W et al. (2009) fMRI at 1.5, 3 and 7 T: characterizing BOLD signal changes. Neuroimage 47:1425-1434.
4. Gati JS, Menon RS et al. (1997) Experimental determination of the bold eld strength dependence in vessels and tissue. Magn Reson Med 38:296-302.
5. Haacke EM, Cheng NY et al. (2005) Imaging iron stores in the brain using magnetic resonance imaging. Magn Reson Med 23:1-25.
6. Anderson LJ et al. (2001) Cardiovascular T2-star (T2*) magnetic resonance for the early diagnosis of myocardial iron overload. Eur Heart J 22:2171-2179.
7. Wood JC et al. (2005) MRI R2 and R2* mapping accurately estimates hepatic iron concentration in transfusion- dependent thalassemia and sickle cell disease patients. Blood, 106:1460-1465.
8. Grandin CB. (2003) Assessment of brain perfusion with MRI: methodology and application to acute stroke. Neuroradiology 45:755-766.
9. Wirestam R et al. (2010) Comparison of quantitative dynamic susceptibility contrast MRI perfusion estimates obtained using different contrast agent administration schemes at 3T.Eur J Radiol 75:86-91.
10. An H, Lin W. (2003) Impact of intravascular signal on quantitative measures of cerebral oxygen extraction and blood volume under normo and hypercapnia conditions using an asymmetric spin echo approach. Magn Reson Med 50:708-716.
11. Frahm J et al. (1998) Direct Flash MR imaging of magnetic field inhomogeneities by gradient compensation. Magn Reson Med 6:474-480.
12. G.E. Hagberg et al. (2002) Real- Time Quantitation of T2* Changes Using Multiecho Planar Imaging and Numerical Methods. Magn Reson Med 48:877-882.
13. O. Wieben, J et al. (2005) Multi-Echo balanced SSFP imaging for iterative Dixon reconstruction. 13th Proceedings of the International Society for Magnetic Resonance in Medicine, Miami, FL, pp: 2386.
14. H. Eggers et al. (2008) Phase and Amplitude Correction in Bipolar Multi-Gradient-Echo Water-Fat Imaging. 16th International Society for Magnetic Resonance in Medicine, Toronto, pp: 1623.
15. S. B. Reeder et al. (2006) Quantification of Hepatic Steatosis with MRI: The Effects of Accurate Fat Spectral Modeling. The 14th International Society for Magnetic Resonance in Medicine, Washington.